machines

MDPI

Article

Research on a Novel Trailing-Edge Winglet with Passive Automatic Angle-of-Attack Adjustment Function

Yun Wang [1,*], Maoyuan Li [1,2] and Xun Li [1]

[1] School of Aeronautical Engineering, Taizhou University, Taizhou 318000, China; li303987792@gmail.com (M.L.); lixun_1981@163.com (X.L.)
[2] Chengdu Aircraft Industrial (Group) Co., Ltd., Chengdu 610092, China
* Correspondence: wangyun66@126.com

Abstract

Low-altitude general aviation aircraft and unmanned aerial vehicles (UAVs) are widely deployed for complex operational tasks, yet low-altitude gusts and crosswind disturbances induce severe airspeed fluctuations, leading to variable lift, unstable flight altitude, and perturbed pitch attitude. Such aerodynamic fluctuations degrade flight smoothness and increase pilot control workload. To mitigate lift and altitude instability under unsteady incoming flow, this paper proposes a novel passive trailing-edge winglet configuration capable of self-regulating wing angle of attack (AOA) without active flight control systems. A quasi-static aerodynamic equilibrium analytical model based on moment balance about the wing pivot axis is established, combined with validated Computational Fluid Dynamics (CFD) simulations to characterize the passive AOA adjustment mechanism and quantify lift variations under velocity perturbations. Results demonstrate that the integrated wing-winglet layout generates passive aerodynamic feedback moments to automatically adjust the wing AOA when freestream speed varies. For airspeed disturbances within ±10% of the cruise velocity (102 m/s, 0.3 Ma), the total lift fluctuation of the wing-winglet assembly is suppressed within ±1.01%, whereas conventional fixed-wing configurations experience lift deviations between −16% and +22% under identical disturbance conditions. Notably, the present study only verifies quasi-static aerodynamic equilibrium under steady inflow; dynamic flight stability, unsteady aerodynamic effects, and stall-limit performance remain unexamined and require further investigation. The core novelty of this design lies in the passive negative-feedback aerodynamic moment generated by the trailing-edge winglet, which decouples fuselage attitude from wing pitching motion and stabilizes equilibrium lift under mild low-altitude gust perturbations.

Keywords: passive aerodynamic control; flight altitude stabilization; trailing-edge winglet; self-adjusting angle of attack; aerodynamic moment equilibrium

Check for updates

Academic Editor: Massimo Sorli

Received: 10 June 2026
Revised: 10 July 2026
Accepted: 20 July 2026
Published: 27 July 2026

Copyright: © 2026 by the authors. Licensee MDPI, Basel, Switzerland. This article is an open access article distributed under the terms and conditions of the Creative Commons Attribution (CC BY) license.

1. Introduction

Sustained lift and attitude stability are critical metrics for aircraft performance: stable aerodynamic loads mitigate turbulence-induced fuselage jitters, improve passenger comfort in civil aircraft, and guarantee reliable low-altitude mission execution. In contrast, unsteady lift caused by atmospheric disturbances triggers altitude and pitch variations, deteriorating flight quality and even triggering catastrophic flight incidents [1]. For conventional fixed-wing aircraft operating at low altitudes, complex ambient airflow continuously alters freestream

velocity, inducing periodic lift fluctuations. Although active flight control surfaces can compensate for altitude deviations, they inevitably introduce fuselage pitching oscillations, sacrificing ride smoothness and increasing continuous control burden for pilots.

Extensive research has addressed gust alleviation and passive lift stabilization, primarily focusing on free-wing architectures and biplane/tandem-wing layouts [2–14]. As early as 1944, Danil R. Z. first patented the free-wing concept and fabricated a small-scale free-wing demonstrator, which exhibited favorable gust rejection via freely pitching wing segments [2]. This milestone work is widely recognized as the foundational exploration of passive load alleviation through pivot-mounted lifting surfaces. Subsequent developments include the 1986 "Scorpion" tilt-fuselage free-wing aircraft, which shortened takeoff distances by decoupling wing and fuselage pitching motions [4]. Brandt et al. optimized free-wing pivot positions and mass distribution, establishing quantitative design guidelines for swept free-wing prototypes [5]. To expand the stall margin of free-wing systems, Sun et al. implemented slotted synthetic jet active flow control on free-wing trailing edges [6]. Nevertheless, conventional free-wing designs rely on large trailing-edge flaps that introduce substantial profile drag and permanent lift loss, limiting overall aerodynamic efficiency under cruise conditions.

Biplane and tandem-wing configurations represent another mainstream route for aerodynamic interference optimization. NASA verified that upper auxiliary lifting surfaces can boost aerodynamic efficiency by up to 13% for biplane layouts [7]. For micro air vehicles operating at low Reynolds numbers, biplane structures suppress flow separation during pitching maneuvers and improve low-speed lift characteristics [8]. Inter-wing downwash from forward lifting surfaces modifies the effective AOA of rear wings to enhance total lift output [10], while closely coupled biplanes deliver superior lift-to-drag ratios at low Reynolds numbers via an optimized aerodynamic interference [14]. Tandem wing layouts further delay trailing-edge separation by accelerating inter-wing airflow, improving overall aerodynamic efficiency across low-speed operating envelopes [11,13].

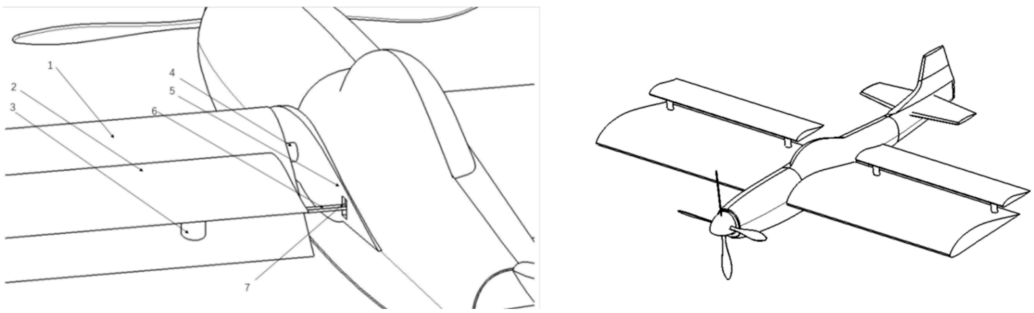
Despite these advances, existing passive gust alleviation schemes fall into two isolated categories: standalone free-wing pivoting designs or rigid fixed biplane/tandem wing layouts. Few architectures integrate the advantages of both mechanisms to achieve passive AOA self-regulation without severe aerodynamic penalties. Recent progress in passive gust load alleviation, aeroelasticity, and adaptive wings further highlights the research gap: most state-of-the-art passive control strategies rely on structural buckling, variable spoilers, or elastic deformation, rather than aerodynamic moment feedback from lightweight trailing-edge auxiliary winglets [15–17]. Classical aircraft stability theory establishes critical distinctions between static moment equilibrium and dynamic flight stability, a separation rarely addressed in prior free-wing and biplane passive control studies [18,19]. Aeroelastic coupling between passive lifting surfaces and fuselage structures also remains insufficiently quantified in low-altitude UAV passive load control research [20].

Against this background, this work proposes a novel pivot-mounted wing integrated with a small trailing-edge winglet, combining the decoupling merits of free-wing pitching and the aerodynamic interference benefits of biplane layouts [21]. The winglet generates velocity-dependent feedback moments about the main wing pivot axis to passively adjust main wing AOA, suppressing lift fluctuations under mild airspeed perturbations and maintaining consistent flight altitude without active control deflection. This study establishes a quasi-static moment equilibrium theoretical framework and validates the lift-stabilization performance via CFD simulations. The manuscript clearly distinguishes quasi-static aerodynamic balance from full dynamic flight stability and discusses the inherent limitations of the proposed passive mechanism to position its contributions within the broader passive aerodynamic control literature.

2. Principle and Structural Design of the Trailing-Edge Winglet System

2.1. Structural Layout of the Passive AOA Adjustment Winglet System

The main wing is articulated to the fuselage via a single-pivot axis located at the main wing aerodynamic center, permitting limited small-amplitude pitching rotation. A compact auxiliary winglet is rigidly mounted on the upper trailing edge of the main wing via support struts. Mechanical limit blocks integrated with linear damping springs constrain the maximum pitching deflection of the main wing to avoid over-rotation under extreme disturbances. The complete assembly and disassembled component layout are illustrated in Figure 1.



(**a**) (**b**)

Figure 1. Proposed trailing-edge winglet passive adjustment system. (**a**) Structural components; (**b**) complete aircraft assembly under cruise configuration.

2.2. Physical Mechanism of Passive AOA Self-Adjustment

Under steady cruise velocity, the entire wing-winglet assembly satisfies static moment equilibrium about the pivot axis. When positive velocity perturbations occur (air speed increases), the lift generated by the trailing-edge winglet rises proportionally, producing an additional counterclockwise moment about the pivot axis. This pitching-down moment reduces the main wing AOA to offset the velocity-induced lift increment, restoring total lift to the baseline cruise value. Conversely, negative velocity perturbations reduce winglet lift and its associated pivot-axis moment, triggering the clockwise main wing rotation to increase AOA and compensate for lift loss. Crucially, all pitching rotation occurs exclusively between the main wing assembly and fuselage; fuselage attitude remains unperturbed during passive AOA regulation. Conventional horizontal tail control authority is fully preserved for pilot manual flight maneuvers, identical to that of standard fixed-wing aircraft. The quasi-static adjustment cycle is visualized in Figure 2.

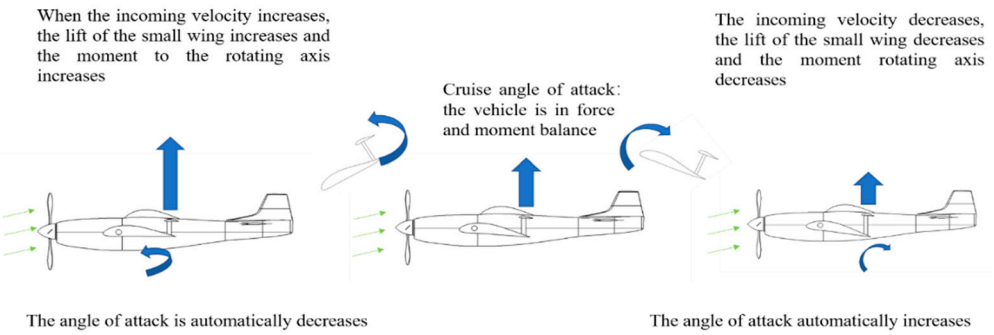


Figure 2. Schematic diagram of the passive self-adjusting angle-of-attack principle under positive/negative velocity perturbations.

The theoretical derivation in this section only characterizes quasi-static aerodynamic moment balance under steady, time-invariant inflow conditions, which cannot validate

the dynamic stability of the wing-fuselage coupled system under transient unsteady gusts [RAR4]. Dynamic stability analysis incorporating pitch damping, aeroelastic coupling, and transient flow effects is beyond the scope of the present quasi-static CFD study and is identified as a key limitation in the subsequent discussion. All conclusions drawn herein are restricted to steady-state equilibrium conditions, consistent with the static force balance derivation in Section 2.3.

Unlike conventional fixed-wing designs where the fuselage center of gravity lies forward of the aircraft's aerodynamic center (requiring negative tail lift for trimming and introducing aerodynamic losses), the proposed pivot-mounted architecture decouples fuselage and wing pitching motions. The fuselage center of gravity can be positioned aft of the pivot axis, and both the main wing, trailing-edge winglet, and horizontal stabilizer generate positive lift under cruise conditions, eliminating trimming drag penalties and improving the overall lift-to-drag ratio. The full force and moment free-body diagram for the wing-winglet assembly under steady cruise is provided in Figure 3, with explicit labeling of all force vectors, moment arms, and load application points to support the analytical equilibrium equations in Section 2.3.

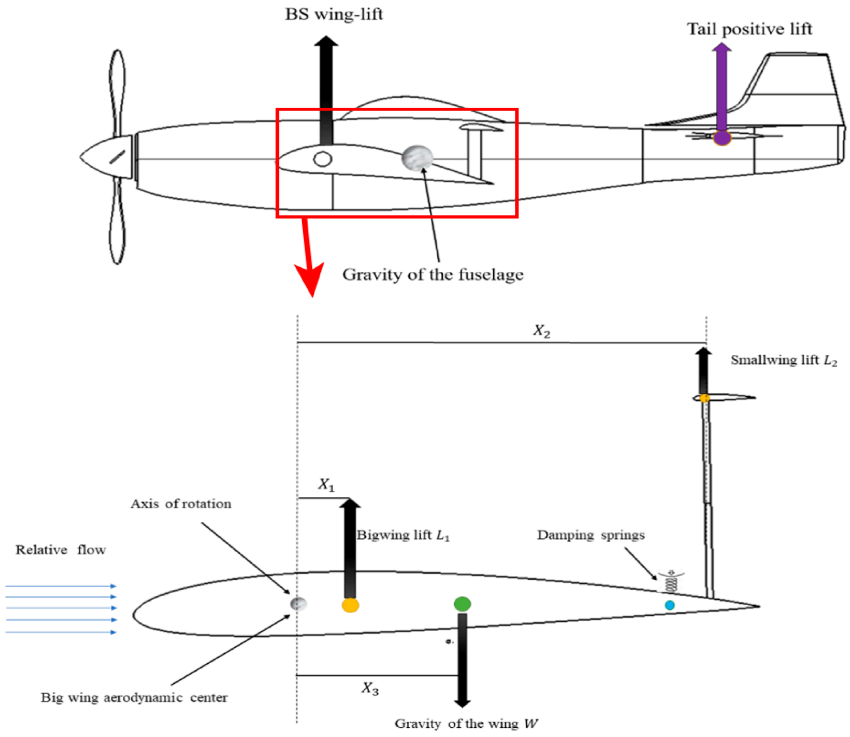


Figure 3. Free body diagram of the integrated wing-winglet structural system under steady cruise flight, annotated with all aerodynamic loads, gravitational forces, moment arms, and pivot axis reference.

2.3. Quasi-Static Lift and Moment Equilibrium Analysis

All aerodynamic moments are defined using standard aerospace terminology: moment about the pivot axis, replacing the non-standard phrase "moment to the rotating axis" used in the initial manuscript (per CSI2, consistent with [18,19]). From the free-body diagram (Figure 3), the loads acting on the wing-winglet assembly include:

Main wing lift L_1: moment arm from main wing aerodynamic center to pivot axis: X_1.

Trailing-edge winglet lift L_2: moment arm from winglet aerodynamic center to pivot axis: X_2.

Gravitational weight of the wing assembly W: moment arm from wing center of gravity to pivot axis: X_3.

At cruise state, the moment can be assumed to be in equilibrium:

$$L_{1(v,\alpha)}X_1 + L_{2(v,\alpha)}X_2 = WX_3 \tag{1}$$

The moment on the rotating shaft $\sum M_0$ is in equilibrium and can be expressed as follows:

$$\sum M_0 = L_{1(v,\alpha)}X_1 + L_{2(v,\alpha)}X_2 - WX_3 = 0 \tag{2}$$

When there is a perturbation in velocity, e.g., $\Delta v > 0$, the increase in velocity causes an increase in lift force ΔL, and the moment at the rotating shaft after the velocity perturbation can be expressed as follows:

$$\left(L_{1(v,\alpha)} + \Delta L_1\right)X_1 + \left(L_{2(v,\alpha)} + \Delta L_2\right)X_2 > WX_3 = L_1X_1 + L_2X_2; \sum M_0 > 0, \tag{3}$$

The wing rotates counterclockwise about its axis, and the AOA of the wing decreases, which reduces the lift of the wing. When the AOA is reduced to α' under the velocity perturbation, the moments of the wing about the axis of rotation are balanced again as follows:

$$L'_{1(v+\Delta v,\alpha')}X_1 + L'_{2(v+\Delta v,\alpha')}X_2 = WX_3 = L_1X_1 + L_2X_2 \tag{4}$$

$$\left(L'_{1(v+\Delta v,\alpha\prime)} - L_{1(v,\alpha)}\right)X_1 + L'_{2(v+\Delta v,\alpha')} - L_{2(v,\alpha)}\Big)X_2 = 0 \tag{5}$$

Considering that wing and winglet use the same wing type, $\mathrm{L} = \frac{1}{2}\rho V^2 C_L S$, the above equations are transformed into the following:

The relationship between the velocity perturbation and AOA adjustment is as follows:

$$\frac{1}{2}\rho V^2 S_1 X_1[(v+\Delta v)^2 C_{L(\alpha')} - v^2 C_{L(\alpha)}] + \frac{1}{2}\rho V^2 S_2 X_2[(v+\Delta v)^2 C_{L(\alpha')} - v^2 C_{L(\alpha)}] = 0 \tag{6}$$

$$\left[\left(v+\Delta v\right)^2 C_{L(\alpha')} - v^2 C_{L(\alpha)}\right] = 0 \tag{7}$$

From the lift coefficient curve $C_L = k\alpha + b$, we have:

$$\frac{(v+\Delta v)^2}{v^2} = \frac{C_{L(\alpha)}}{C_{L(\alpha')}} \rightarrow \frac{(v+\Delta v)^2}{v^2} = \frac{k\alpha + b}{k\alpha' + b} \tag{8}$$

Therefore, when a disturbance occurs within a certain range of speed, there is always an adjustment angle of attack for the wing that can balance the torque of the wing to the rotor shaft at the angle of attack again.

According to the NACA 2412 airfoil lift coefficient, we can deduce the following:

$$C_L = k\alpha + b = 0.07643\alpha + 0.30895. \tag{9}$$

when the speed disturbance is positive. Under normal circumstances, airflow disturbances cause variations in airfoil airspeed within 10%. Taking a low-altitude flight at 0.3 Ma (102 m/s) as an example, when airspeed disturbance increases by10%, lift increases by 21%. The relationship between the angle of attack (α) before disturbance and the angle of attack (α') after disturbance when lift stabilizes is expressed as follows:

$$\frac{(v+\Delta v)^2}{v^2} = \frac{(102+10.2)^2}{102^2} = 1.21 \rightarrow \frac{k\alpha + b}{k\alpha' + b} = 1.21, \tag{10}$$

As an example, consider $\alpha = 8^\circ$. We found that $\alpha' = 5.91^\circ$ at the moment the balanced state is reached, and the angle of attack of the big and winglet can be automatically adjusted

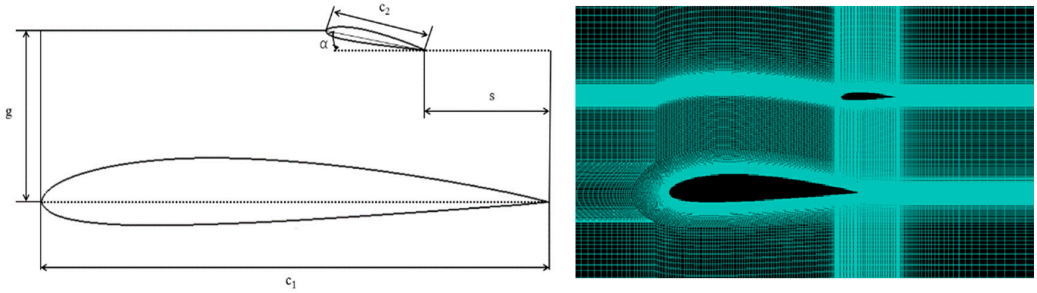
to the angle of attack. And similarly, when the speed disturbance is negative and the magnitude is less than 10%, we found that $\alpha' = 10.82^\circ$ and the moment reaches the balanced state again.

This self-adjusting ability allows the wing trailing-edge winglets to change the AOA with the change in speed and spontaneously achieve the self-balancing state. This self-balancing ability can ensure the stability of the aircraft's body posture and enhance the smoothness of the flight.

3. Aerodynamic CFD Simulation of the Trailing-Edge Winglet Configuration

3.1. Computational Model and Geometric Parameters

The physical model of the wing trailing-edge winglets is shown in Figure 4a. Both the wing and the winglet employ the commonly used NACA2412 airfoil, the parameters of which are listed in Table 1. Figure 4b displays the mesh grid diagram.



(**a**) (**b**)

Figure 4. Aerodynamic simulation model of the wing trailing-edge winglet. (**a**) Physical model; (**b**) mesh generation.

Table 1. Geometric design parameters of the main wing and trailing-edge winglet.

Parameter	Main Wing	Trailing-Edge Winglet
Airfoil Profile	NACA 2412	NACA 2412
Root Chord Length	1.0 m	0.1 m
Tip Chord Length	1.0 m	0.1 m
Half-Span Length	2.5 m	2.5 m
Aspect Ratio	2.5	25
Planform Area	2.5 m^2	0.25 m^2

Typically, the vertical offset between the winglet and main wing is set to 40% of the main wing chord length, and the chord ratio of winglet to main wing is fixed at 0.1. The pivot axis is positioned at the main wing aerodynamic center; counterclockwise moments about the pivot correspond to pitch-down (an AOA reduction), and clockwise moments correspond to pitch-up (an AOA increase).

3.2. Full CFD Numerical Setup

Turbulence closure: A standard SST k−ω model is used, which is suitable for low-speed airfoil boundary layer separation prediction.

Boundary conditions: Wing and winglet surfaces are assigned a no-slip wall; far-field upstream/upper/lower boundaries are set to velocity inlet v = 102 m/s and T = 300 K; and the downstream trailing-edge boundary is set to the pressure outlet.

Convergence criteria: This includes residual thresholds $<10^{-6}$ for continuity, momentum, and turbulence variables; monitored lift/moment coefficients stabilized with relative variation <0.1% over 500 iterative steps.

Mesh independence test: Three-mesh refinement levels (coarse/medium/fine) were evaluated; the medium mesh with 2.1 million polyhedral cells delivers converged C_L and C_M results with <1% deviation relative to the fine mesh, and this was adopted for all subsequent simulations.

Modeling verification: Figure 5 shows the calculated and experimental pressure coefficient curve of the NACA2412 airfoil at 10 angles of attack. Table 2 shows the comparison of the simulation results of the airfoil lift coefficient with the angle of attack and the experimental value. According to Figure 5 and Table 2, the simulation calculation results of the surface pressure coefficient with the angle of attack 10 and the change in lift coefficient are similar to the research results and the calculation error meets the requirements of the flow field calculation.

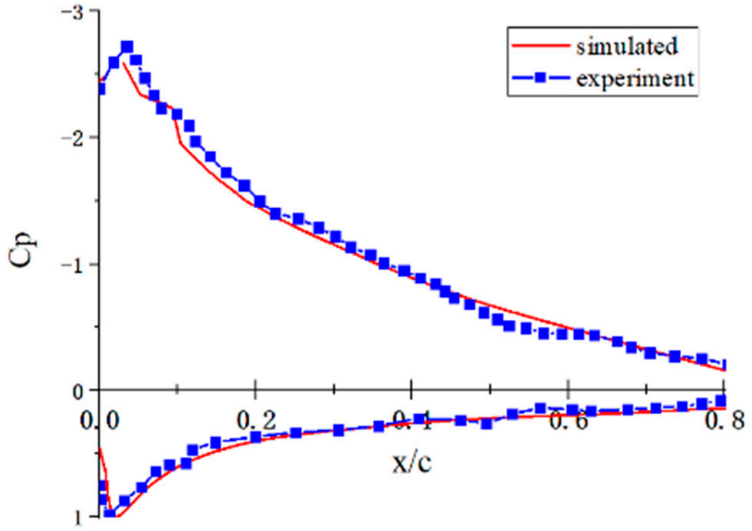


Figure 5. Comparison of simulation and experimental values of airfoil surface pressure coefficient.

Table 2. Comparison of simulated and experimental lift coefficients for the NACA 2412 airfoil across angles of attack.

Angle of Attack (°)	Experimental C_L	Simulated C_L	Absolute Deviation (%)
0	0.20514	0.20443	0.34611
2	0.43085	0.41150	4.49112
4	0.75574	0.61669	18.39918
6	0.83953	0.81590	2.81467
8	0.97253	1.00600	3.44154
10	1.15722	1.18160	2.10677

3.3. Baseline CFD Flow Field Results

Figure 6 presents the static pressure contour of the integrated wing-winglet assembly under cruise conditions v = 102 m/s, $\alpha = 8°$, illustrating low-pressure suction zones on the upper surfaces of both lifting components that generate the primary aerodynamic loads driving pivot-axis moment feedback.

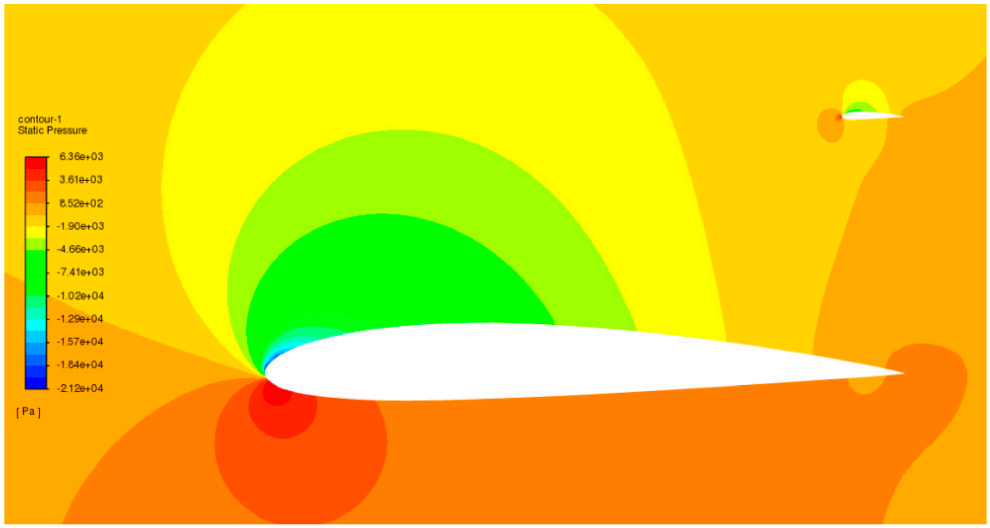


Figure 6. Wing trailing-edge winglet pressure cloud map (r = 0.1, g = 0.4, AOA = 8°, 102 m/s).

Figure 6 Static pressure contour of the trailing-edge winglet-integrated configuration at cruise speed v = 102 m/s and baseline AOA = 8°.

4. Results and Discussion

4.1. Variation in Wing Aerodynamic Torque Under Different Working Conditions

The aerodynamic moment of the wing to the rotor shaft (which is also the focus of the wing) with varying velocity and AOA is shown in Figure 7a. Because the rotating shaft is set in focus, as expected, the anticlockwise moment of the wing on the rotor shaft basically does not change with AOA at the same velocity. But it does increase with the increase in velocity and decreases with the decrease in velocity. From Figure 7b, it can be seen that the anticlockwise moment of the winglet acting on the rotor shaft increases when the velocity or AOA increases.

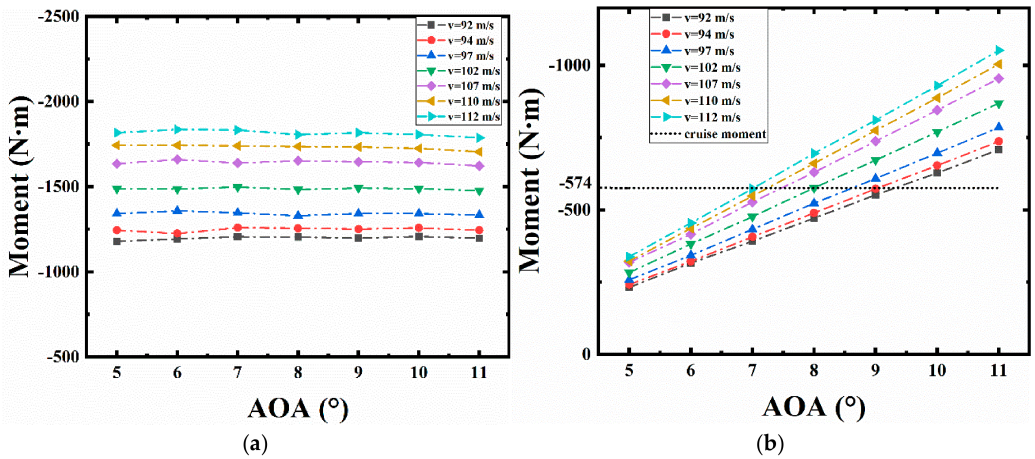


Figure 7. Variation in aerodynamic moments about the pivot axis with flight velocity and angle of attack. (**a**) Moment contribution from the main wing; (**b**) moment contribution from the trailing-edge winglet.

Figure 7 plots the aerodynamic moment around the pivot axis for the main wing and trailing-edge winglet across flight speeds (92–112 m/s) and AOA (5–11°). All moment values follow a unified sign convention: counterclockwise pitching-down moments are assigned negative values, whereas clockwise pitching-up moments have positive values.

Main wing moment (Figure 7a): Since the pivot axis coincides with the main wing aerodynamic center, the main wing moment exhibits negligible sensitivity to AOA at a fixed velocity and increases monotonically with rising freestream speed.

Winglet moment (Figure 7b): The winglet-generated counterclockwise moment rises linearly with both velocity and AOA, forming the core negative-feedback moment driving passive AOA adjustment. The horizontal dotted line denotes the baseline cruise equilibrium moment at v = 102 m/s, $\alpha = 8°$.

Unified sign convention: Counterclockwise pitch-down moments = negative values; clockwise pitch-up moments = positive values. The dotted line indicates the baseline cruise equilibrium moment.

4.2. Quasi-Static Equilibrium AOA Following Velocity Perturbations

The winglet is rigidly coupled to the main wing, so both surfaces share identical AOA and freestream velocity. Positive velocity perturbations amplify the winglet counterclockwise moment, pitching the main wing down to reduce AOA until incremental total moments around the pivot axis return to zero, defining the new equilibrium AOA. Simulations at ±5 m/s velocity offset the cruise speed of v = 102 m/s and $\alpha = 8°$, yielding equilibrium AOA values of 6.05° (+5 m/s disturbance) and 10.25° (−5 m/s disturbance), as visualized in Figure 8. The vertical intersection of the total incremental moment curve with the zero-moment horizontal axis marks the balanced AOA for each perturbation case.

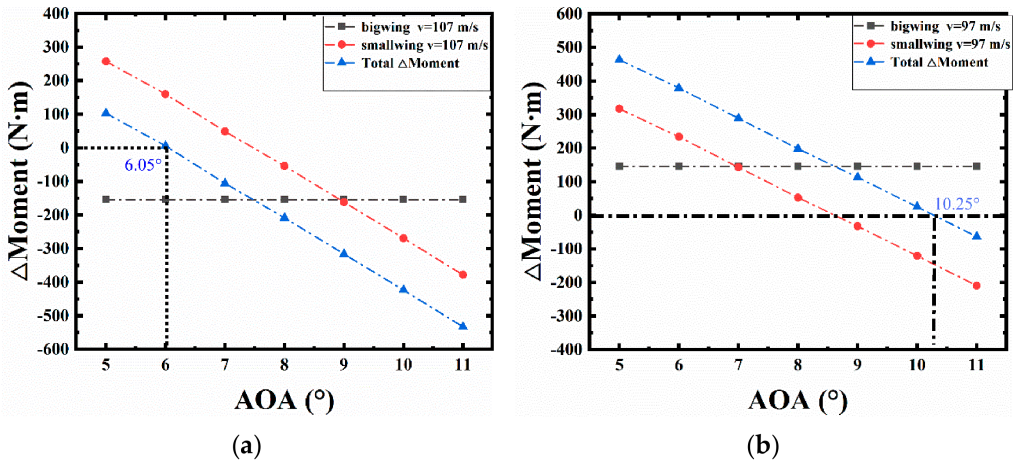


Figure 8. Determination of quasi-static equilibrium angle of attack under ±5 m/s velocity perturbations relative to cruise speed (102 m/s, initial AOA = 8°). (**a**) Figure 5, m/s; (**b**) freestream velocity decreased by 5 m/s.

The intersection of a total incremental moment curve with a zero-moment axis denotes balanced AOA.

4.3. Equilibrium AOA Adjustment with Damping Spring Limiter Effects

To suppress excessive pitching deflection under abrupt gust transients, mechanical limit blocks fitted with linear damping springs are integrated into the structural design. The spring generates a restoring torque proportional to the wing's pitching, which is offset from the baseline cruise AOA, reducing the magnitude of passive AOA adjustment relative to the undamped theoretical case. Simulation parameters are as follows: main wing chord = 1 m; pivot at 23.22% chord (aerodynamic center); spring mounting at 90% chord; stiffness k = 8578 N/m; and this produces 100 N·m restoring torque per 1° AOA deviation. Under ±5 m/s velocity perturbations, the damped equilibrium AOA shifts to

6.98° (+5 m/s) and 9.05° (−5 m/s), demonstrating effective attenuation of pitching motion while retaining lift stabilization capability (Figure 9).

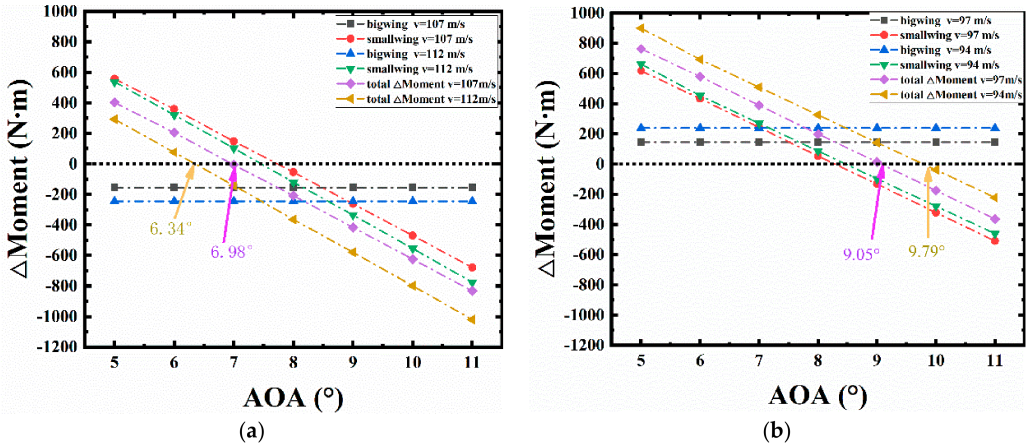


Figure 9. Damped equilibrium wing angle of attack under ±5 m/s velocity perturbations, accounting for torque restored from the pitching limit damping spring (cruise speed = 102 m/s; initial AOA = 8°). (**a**) Velocity increases; (**b**) velocity decreases.

4.4. Lift Stabilization Performance Under Velocity Disturbances

The primary performance metric of the proposed configuration is the suppression of total lift fluctuations under airspeed perturbations. Figure 10 and Table 3 quantify lift deviations relative to the baseline cruise lift (23,405.78 N) for velocity offsets ranging from −8 m/s to +10 m/s. Figure 10 compares a conventional fixed-wing layout and the novel passive adjustment wing-winglet assembly. Figure 10b explicitly plots the percentage lift variation for both the conventional fixed-wing and novel wing-winglet assembly to quantify the relative improvement.

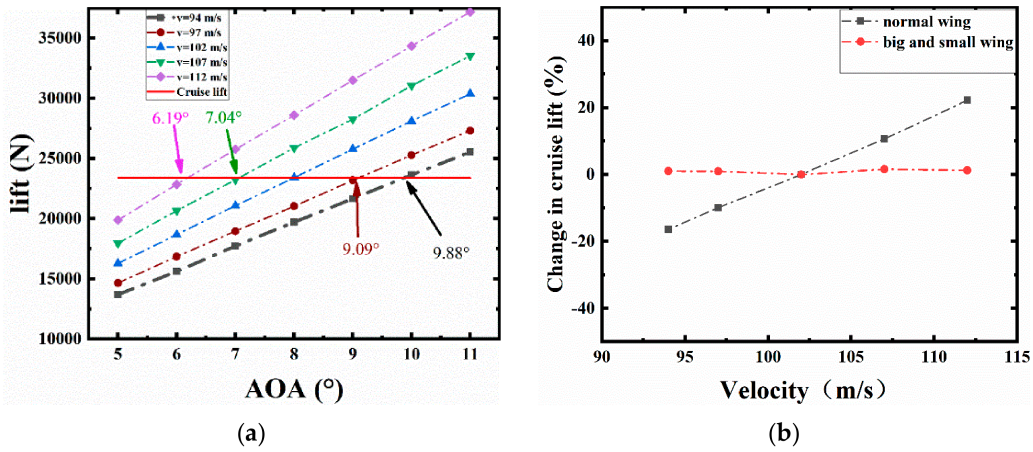


Figure 10. Wing lift stabilization performance of the proposed trailing-edge winglet configuration. (**a**) The equilibrium AOA required to maintain constant cruise lift across varying flight speeds. (**b**) percentage change in the total lift relative to the baseline cruise condition.

Conventional fixed-wing design: Lift variation ranges from −16% to +22% over the tested velocity envelope, inducing severe altitude and pitch oscillations.

Passive trailing-edge winglet design: Total lift deviation is constrained within ±1.01% of cruise lift across all perturbations, eliminating large altitude excursions.

Table 3. Comparison of ideal constant-lift AOA, damped self-adjusted equilibrium AOA, and corresponding total lift deviation relative to baseline cruise lift.

Velocity Perturbation	Ideal Lift-Constant AOA (°)	Damped Self-Adjusted AOA (°)	Stabilized Total Lift (N)	Relative Lift Deviation (%)
+10 m/s (112 m/s)	6.19	6.34	23,640.95	+1.01
+5 m/s (107 m/s)	7.04	6.98	23,181.08	−0.96
Baseline (102 m/s)	8.00	8.00	23,405.78	0.00
−5 m/s (97 m/s)	9.09	9.05	23,286.69	−0.51
−8 m/s (94 m/s)	9.88	9.79	23,221.52	−0.79

4.5. Critical Discussion of Study Limitations

Quasi-static vs. Dynamic Stability Limitation: All simulations assume a steady, time-invariant inflow and only verify static moment equilibrium. This work does not analyze transient dynamic stability, pitch damping, aeroelastic flutter, or unsteady vortex shedding under rapidly evolving gusts. A dynamic flight stability assessment via time-domain CFD or flight dynamics modeling [18,19] is required to validate full flight-envelope performance.

Disturbance Envelope Restriction: Results are only valid for mild-velocity perturbations within ±10% of cruise speed. Performance under large-amplitude gusts, near-stall AOA conditions, and crosswind disturbances is uncharacterized; flow separation at extreme AOA degrades the linear moment feedback mechanism and breaks lift stabilization.

Absence of Experimental Validation: All conclusions are derived from numerical CFD simulations. Wind-tunnel scale-model testing or flight prototype trials are necessary to eliminate numerical modeling uncertainties and validate real-world mechanical friction, spring damping, and structural deformation effects.

Comparative Analysis with Alternative Passive Control: The proposed design is qualitatively compared to free-wing and biplane layouts in the introduction; quantitative benchmarking against modern passive gust alleviation technologies (buckling structures and passive spoilers [15,16]) is recommended for follow-up research.

5. Conclusions

This paper addresses lift and altitude instability problems of low-altitude UAVs and general aviation aircraft under mild gust disturbances by proposing a passive trailing-edge winglet architecture with self-adjusting AOA capability, designed to suppress lift fluctuations without active flight control surfaces. A quasi-static moment equilibrium theoretical framework is established, and validated CFD simulations are conducted to quantify the passive aerodynamic feedback performance of the wing-winglet assembly. Key conclusions strictly limited to the findings supported by the present steady-state numerical analysis are summarized as follows:

5.1. Under steady inflow with mild velocity perturbations within ±10% of cruise speed (102 m/s, 0.3 Ma), the trailing-edge winglet generates velocity-dependent aerodynamic feedback moments about the main wing pivot axis, driving small-amplitude passive pitching rotation to achieve a new quasi-static moment equilibrium AOA. The magnitude of AOA adjustment is attenuated by the linear damping spring fitted to the pitching limit blocks; increasing the spring stiffness reduces the range of passive AOA deflection.

5.2. For all tested velocity perturbations (−8 m/s to +10 m/s), the damped passive adjustment mechanism restricts total wing-winglet lift deviation within ±1.01% relative to the baseline cruise lift, in stark contrast to conventional fixed-wing aircraft, which experience lift variations between −16% and +22% under identical disturbance conditions. This substantial reduction in lift fluctuation mitigates altitude and pitch attitude oscillations, lowering pilot control workload and improving low-altitude flight smoothness.

5.3. The integrated layout decouples the fuselage attitude from wing pitching motion, eliminating the need for a negative trimming lift on horizontal stabilizers under cruise conditions and improving overall aerodynamic efficiency compared to traditional free-wing designs with large trailing-edge drag penalties.

Study Limitations and Future Research Outlook: The conclusions above are restricted to steady quasi-static flow conditions; the manuscript does not provide evidence for dynamic flight stability, unsteady gust responses, near-stall performance, or physical experimental validation. Future work will incorporate transient CFD dynamic stability analysis, wind-tunnel model testing, and quantitative comparative studies with state-of-the-art passive gust load alleviation architectures to resolve the identified limitations.

Academic Contribution to the Existing Literature: This study complements existing passive aerodynamic control research by proposing a lightweight trailing-edge winglet feedback mechanism that merges the decoupling advantages of free-wing pivoting and the aerodynamic interference benefits of biplane layouts. It establishes a clear theoretical distinction between quasi-static moment equilibrium and dynamic flight stability—an oversight common in prior free-wing and adaptive-wing publications—and provides a fully validated numerical benchmark for passive lift stabilization design targeted at low-altitude UAV applications.

Author Contributions: Y.W.: Conceptualization, manuscript writing; M.L.: Computational simulation and validation; X.L.: English translation, language polishing and figure preparation. All authors have read and agreed to the published version of the manuscript.

Funding: This research received no external funding.

Data Availability Statement: The data supporting the results of this study are available.

Conflicts of Interest: Author MaoYuan Li was employed by the Chengdu Aircraft Industrial (Group) Co., Ltd. The remaining authors declare that the research was conducted in the absence of any commercial or financial relationships that could be construed as a potential conflict of interest.

References

1. Yuefeng, L.; Kai, Z.; Yue, C.; Ying, S. Correlation study of low-altitude turbulence in civil aircraft with geographical environmental factor. *Beijing Da Xue Xue Bao* **2019**, *55*, 683–691. [CrossRef]
2. Danil, R.Z. Airplane with Nonstalling and Glide Angle Control Characteristics. U.S. Patent 2,347,230, 1944.
3. Ro, K.; Park, W.; Kuk, T.; Kamman, J. Flight testing of a free-wing tilt-body aircraft. In Proceedings of the AIAA Infotech@Aerospace Conference, Atlanta, GO, USA, 20–22 April 2010; p. AIAA 2010-3449.
4. Chen, W.; Barlow, J. An ultralight freewing aircraft design study. In Proceedings of the AIAA Guidance, Navigation and Control Conference, Hilton Head Island, SC, USA, 10–12 August 1992; p. AIAA 92-4194.
5. Brandt, J.; Neuland, R.; VanDeRoer, N. Design, build, and testing of a swept back free-wing aircraft. In Proceedings of the 51st AIAA Aerospace Sciences Meeting, Grapevine, TX, USA, 7–10 January 2013; p. AIAA 2013-0138.
6. Shengshu, S.; Yunsong, G.; Yongliang, C.; Xiong, Z. Separation flow control on free-wing with beveled-slit-synthetic-jet at low Reynolds numbers. *Acta Aerodyn. Sin.* **2017**, *35*, 277–282. [CrossRef]
7. Ball, P.; Smith, H. Aerodynamic characteristics of biplanes with winglets. *J. Aircr.* **1987**, *24*, 518–522. [CrossRef]
8. Thipyopas, C.; Moschetta, J. A fixed-wing biplane MAV for low speed missions. *Int. J. Micro Air Veh.* **2009**, *1*, 13–33. [CrossRef]
9. Wang, J.; Liu, P.; Chin, C.; He, G. Numerical investigation of auto-pitch wing-in-ground effect oscillating foil propulsor. *Appl. Ocean Res.* **2019**, *89*, 71–84. [CrossRef]
10. Guo, R.; Bai, Y.; Pei, X.; Lai, Z. Numerical investigation of aerodynamics and wake on biplane airfoils at high angles of attack. *Int. J. Mech. Sci.* **2021**, *205*, 106606. [CrossRef]
11. Hua, R.; Ye, Z. Experimental investigation on the aerodynamic characteristics of row-biplane aircraft. *J. Exp. Mech.* **2013**, *28*, 453–459. [CrossRef]
12. Hua, R.; Ye, Z. Research on effective aerodynamic configuration of row inflatable wings. *Acta Aerodyn. Sin.* **2012**, *30*, 184–191.
13. Zhang, Q.; Ye, Z. Computational Investigations for Aerodynamic Characteristic Analysis of Low Reynolds Number Doubly-Tandem Wing Configurations. *Eng. Mech.* **2019**, *36*, 244–256.

14. Luo, L.; Jiang, C.; Gao, Z.; Lee, C. Aerodynamic Interference and Reynolds Number Effects of Low-Speed Close-Coupled Biplanes. *J. Aerosp. Eng.* **2020**, *33*, 04020026. [CrossRef]
15. Wheatcroft, E.D.; Mahadik, Y.; Groh, R.M.J.; Schenk, M. Gust load alleviation performance of a passively actuated spoiler: An aircraft-scale aeroelastic study. *Aeronaut. J.* **2025**, *130*, 1268–1289. [CrossRef]
16. Toffol, F.; Bisagni, C. Gust Load Passive Alleviation by Means of Buckling-Driven Structures. In Proceedings of the 34th International Council of the Aeronautical Sciences (ICAS 2024), Florence, Italy, 9–13 September 2024. Paper No. ICAS2024_0147.
17. He, S.; Guo, S.; Liu, Y.; Luo, W. Passive gust alleviation of a flying-wing aircraft by analysis and wind-tunnel test of a scaled model in dynamic similarity. *Aerosp. Sci. Technol.* **2021**, *113*, 106689. [CrossRef]
18. Etkin, B.; Reid, L.D. *Dynamics of Flight: Stability and Control*, 3rd ed.; John Wiley & Sons: Hoboken, NJ, USA, 1996; ISBN 9780471034186.
19. Stevens, B.L.; Lewis, F.L.; Johnson, E.N. *Aircraft Control and Simulation: Dynamics, Controls Design, and Autonomous Systems*, 3rd ed.; John Wiley & Sons: Hoboken, NJ, USA, 2015. [CrossRef]
20. Wright, J.R.; Cooper, J.E. *Introduction to Aircraft Aeroelasticity and Loads*, 2nd ed.; John Wiley & Sons: Hoboken, NJ, USA, 2015. [CrossRef]
21. Wang, Y.; Li, M.; Li, Z.; Zhao, Y.; Li, X. A Kind of Wing That Can Automatically Adjust the Magnitude of the Angle of Attack. Chinese Invention Patent No. 202011560086.5, 12 August 2022.

Disclaimer/Publisher's Note: The statements, opinions and data contained in all publications are solely those of the individual author(s) and contributor(s) and not of MDPI and/or the editor(s). MDPI and/or the editor(s) disclaim responsibility for any injury to people or property resulting from any ideas, methods, instructions or products referred to in the content.